Self-assembly of a patterned hydrophobic-hydrophilic surface by soft segment microphase separation in a segmented polyurethane: Combined experimental study and molecular dynamics simulation

Helma Vakili[a], Mohsen Mohseni [a*], Hesam Makki [a*], Hossein Yahyaei[a], Hossin Ghanbari[b], Alba González[c], Lourdes Irusta[c]

[a] Amirkabir University of Technology, Department of Polymer and Color Engineering, 424 Hafez Ave., Tehran, Iran

[b] Department of Medical Nanotechnology, School of Advanced Technologies in Medicine, Tehran University of Medical Sciences (TUMS), Italia Street, Tehran, Iran

[c] POLYMAT, Department of Polymer Science and Technology, University of the Basque Country (UPV/EHU), Avda. Tolosa 72, Donostia-San Sebastian 20018, Spain

[*] **Corresponding authors:**

Mohsen Mohseni, Phone: +9821 6454 2441, E-mail: mmohseni@aut.ac.ir

Hesam Makki, Phone: +9821 6454 2434, E-mail: hmakki@aut.ac.ir

Abstract

Designing surfaces with patterns of varying wettability is of significant importance for many applications. This fascinating feature is inspired from nature where it is absolutely vital for survival of some living creatures. This research shows that an inherent incompatibility between different soft segments of segmented polyurethanes can play a pivotal role in designing such surfaces. We employed coarse-grained molecular dynamics (CG MD) simulations as well as experimental techniques to illustrate the microphase separation between soft segments with significantly different wettability. We started with poly(hexamethylene carbonate) polyurethane and partially replaced the polycarbonate diol (PC), the hydrophobic soft segment, with poly (ethylene glycol) (PEG), the superhydrophilic soft segment. Our simulation shows that a clear microphase separation between PC and PEG exists. This led to a core-shell structure in which the hard segments are squeezed between two incompatible soft segments. Experimental analyses, e.g., Fourier-transform infrared spectroscopy (FTIR), atomic force microscopy (AFM), differential scanning calorimetry (DSC) and dynamic mechanical thermal analysis (DMTA) merely confirmed the soft segment phase separation. Our combined simulation and experimental analyses showed that there is a concurrent phase mixing of hard/soft segments with phase separation between soft segments. Moreover, the CG MD simulations elucidated the evolution of microphase organization as the polymerization proceeds and our further analysis shed light on the microarchitecture of the individual PU chains.

Keywords: Polyurethane, Polyethylene glycol (PEG), Phase separation, Coarse grained molecular dynamics simulation

Introduction

There are several designed patterned surfaces with different wettability in nature like some insects and plants such as desert beetles and Nepenthes pitcher plant[1]. The nature has inspired scientists to develop patterned surfaces for different applications such as microfluidic channels[2], cell microarrays[3], lithographic printing[4], fog collection[5], patterning textiles[6], self-assembly of microchips[7], etc. However creating such surfaces with designed wettability is not always straightforward. There are several ways to develop surfaces with patterned wettability such as microwave plasma enhanced chemical vapor deposition, UV radiation[3] and surface modification through polydopamine[8], etc. Therefore, finding an easy-fabrication method to develop surface structured materials with different wettability is still a challenge. Incompatibility between the chemically linked segments of PU is a low cost and easy-fabricating method to develop such surfaces with patterned wettability. These chemically bonded materials provide unique microphase morphology[9].

An important characteristic of segmented PU is the microphase separation between different segments due to their inherent incompatibility[10-13]. In segmented polyurethanes, the soft segments consist of macrodiols which provides elasticity[13], and the hard segment, the rigid part, is composed of the diisocynate and chain extenders[14]. These hard and soft segments can act together as chemically linked materials[15]. There is a common knowledge that the degree of compatibility between the hard and soft segments, determines the degree of microphase separation of PU[16-18]. It has been demonstrated that soft segment chemistry plays an effective role in phase organization of PU[19].Thus, the incorporation of different chemical components in PU structure can promote or prevent the microphase separation[20]. In

fact, proper selection of the constituents and their relative composition could lead to PU with desired microstructure and characteristics[21, 22].

There is an extensive record of the effect of microphase separation on the final properties of PU in the literature. For instance, Hsu et al.[23] showed that biological response of the biomaterials deeply depends on their nanophase separation and Choi et al.[24] proved that oxidative biostability is related to phase separation in polydimethylsiloxane (PDMS) based PUs. Eceiza et al.[25] declared that in some polycarbonate based PUs, in spite of increasing the hard segment, the tensile strength decreases due to increase of phase mixing. However, to the best of our knowledge, only a limited number of researches highlighted the effect of soft segment microphase separation on the final properties of PU. Trinca et al.[26] obtained a heterogeneous PU structure by incorporation of different macrodiols, i.e. PLLA (poly(L-lactide)), PTMC (Poly(trimethylene carbonate) and PEG. They showed that the macrodiol composition affects the morphology and properties of the synthesized PU. Hernandez et al.[19] quantified the degree of phase separation for a series of PUs and emphasized on the considerable role of soft segment on the microphase separation in systems containing the same hard segment. Wenning et al.[27] correlated the miscibility of the reactants with the phase behavior during the reaction. They confirmed that sometimes phase separation is a result of incompatibility between two soft segments, not hard and soft segment segregation in PUs. Despite the observation of this interesting phenomenon, no certain interpretation of such occurrence is yet provided.

There are several experimental methods to study the phase organization of segmented PUs, e.g., FTIR, AFM, DSC and X-ray photoelectron spectroscopy (XPS). These methods are often intended to distinguish hard and soft segments in PU system, while it is usually difficult to track phase separation between different soft segments due to very similar physical properties of them. Therefore, we employed a CG MD method to simulate the synthesis and characterization of our PU systems in parallel with the experimental study. Simulation techniques showed a remarkable capability with respect to predicting phase organization of PU systems[28-30]. In fact, MD methods are fully capable of directly observing the microstructure change of complex soft matters, e.g., segmented PU, as a function of time. Yildirim et al.[31] investigated the effect of intersegmental interactions on the phase separation of PUs containing two soft segments by means of Dissipative Particle Dynamics (DPD) simulations. They showed that using hydrophobic soft segments leads to more pronounce phase separation than employing the hydrophilic ones. Wang et al.[32] studied the influence of fluorine content on the microphase separation between hard and soft segments in fluorinated PUs by means of both FTIR and MD simulations. They found that increasing the fluorine content of soft segments leads to PUs with more phase mixed structures. Haddadi-Asl et al.[33, 34] applied MD simulations in combination with experimental techniques to study the intersegmental interactions of PUs based on poly (tetramethylene ether) glycol (PTMG) and polycaprolactone (PCL). They quantified extent and kinetics of micro-phase separation.

We have fabricated microstructure-patterned surfaces with different wettability by means of controlling the microphase separation of the superhydrophilic and hydrophobic components of PU. Ease of fabrication is a superior advantage of this method. Moreover, we have applied MD simulation as a powerful tool to study the regions that experimental techniques are not solely capable of a full investigation. In this study, we started with polyhexamethylene carbonate urethane and partially replaced the PC, a hydrophobic polymer, with PEG, a superhydrophilic polymer, to illustrate the effect of soft segments incompatibility on the PU surface microstructure by means of CG MD simulation as well as experimental techniques. We modified

our recent step-growth polymerization simulation method [35], which was designed to build up thermoset PU networks, in order to synthetize and analyze the thermoplastic segmented PU structures.

Experimental

1. Materials

Polyhexamethylene carbonate diol (PC) (M_w 2000 g/mol, UBE Chemical Corporation) and Poly(ethylene glycol) (PEG) (M_w 2000 g/mol, Merck) as the macrodiols, were dried under vacuum for 24 h at 70 °C before use. Hexamethylene diisocyanate (HDI), Dibutyltin dilaurate (DBTDL) were purchased from Sigma Aldrich and used as received. 1,4-Butanediol (BD) as chain extender was purchased from Sigma Aldrich, distilled and dried over 4 Å molecular sieves. Dimethyl formamide (DMF) as the solvent was obtained from Panreac and dried over 4 Å molecular sieves, before use. Methanol was obtained from Panreac, too.

2. Synthesis

The molar ratio of macrodiol, HDI and BD were 1:3:2, respectively. The synthesis was performed using a two-step procedure. In the first step, the solution of macrodiols in DMF and HDI were reacted in 80 °C for three hours under nitrogen atmosphere. After synthesis of the prepolymer, in the second step BD was added dropwise and the reaction continues until the isocyanate peak in the FTIR spectra at 2270 cm^{-1} disappears. The final solution was precipitated in methanol to remove the unreacted and low molecular weight species. Then dissolved in DMF again, casted in Teflon molds and dried at 85 °C for 24 hours. The samples were finally removed from the Teflon molds and kept in desiccator. The synthesis procedure and the formulations of synthesized PUs are illustrated in *Figure 1* and *Table 1*, respectively.

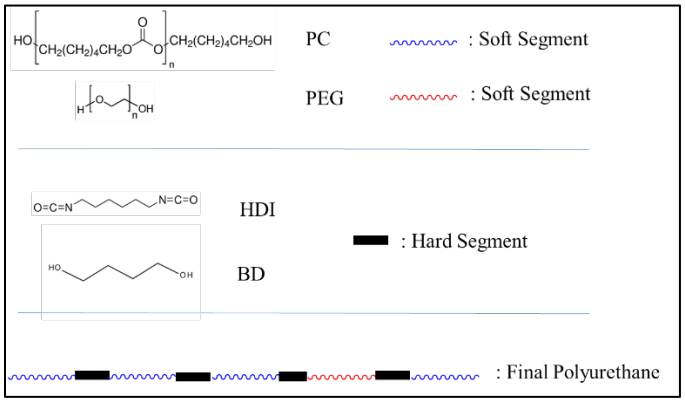

Figure 1. Schematic of experimental procedure.

Table 1. The synthesized polyurethane formulations.

Sample	PEG/PC weight ratio
PEG 0%	0/100
PEG 10%	10/90
PEG 20%	20/80
PEG 30%	30/70

3. Characterization

FTIR spectra were recorded on Nicolet 6700 FTIR spectrometer with 10 scans at a resolution of 4 cm^{-1} for wavelength range of 400 cm^{-1} to 4000 cm^{-1}.

The number-average molar mass (M_n), weight-average molar mass (M_w) and polydispersity index (PDI=M_w/M_n) were determined using gel permeation chromatography (GPC) performed on PL-GPC 50 (Agilent Technologies). DMF (1 mL/min) was used as solvent.

AFM was performed with an AFM Dimension ICON (Bruker) equipment in tapping mode by tips Tesp-v2 (Spring Const.: 37 N/m, Resonant Freq.: 320 khz) at room temperature.

DSC experiments were conducted by TGA Q500, TA Instrument, from -80 to 200 °C at a constant heating rate of 10 °C min^{-1} under nitrogen flow.

A DMTA, Triton 2000 DMA from Triton Technology, was used in tension deformation mode to carry out dynamic mechanical thermal analysis. The samples were heated from −100 ºC to 80 ºC at a constant heating rate of 4 ºC/min and frequencies of 1 Hz. These tests were performed at low strain amplitudes ensuring a linear viscoelastic response. These measurements allowed detecting the glass transition temperature, T_g, given by a maximum peak in loss tangent, tan δ.

X-ray diffraction (XRD) was applied to identify the changes in the degree of crystallinity. An EQUINOX3000 Intel instrument with Cu Kα source operating at a voltage of 40 kV and a current of 40 mA was used. The samples were scanned at 10°/min.

4. Molecular Dynamics Simulations

4.1 Synthesis simulations

We employed a CG MD method, based on the Martini model[36], to simulate the PU synthesis under similar conditions, as in experiment. Note that this CG MD method has been developed and used to study crosslinked PU structures in a preceding paper[35] and this time, we updated it for thermoplastic PU systems. We followed a similar parametrization method, as explained in the preceding paper, based on mapping Martini beads from atomistic structures, see Figure *2* and Table *2*. A detailed explanation about CG parametrization is provided in supporting information, SI (Table S1 and S2).

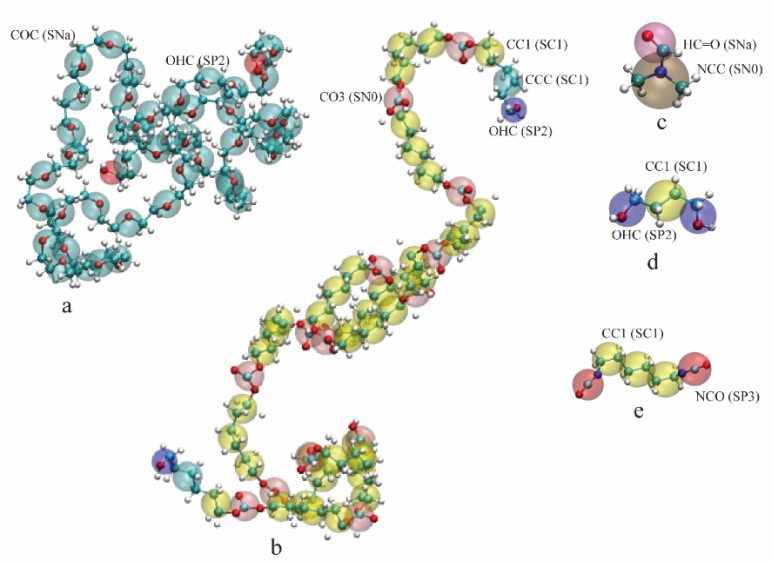

Figure 2. CG mapping of the materials based on MARTINI method. Blue, white, cyan and red colors are assigned to nitrogen, hydrogen, carbon and oxygen, respectively. a, b, c, d and e materials are represented in Table 2.

Table 2. Bead labeling of the materials based on MARTINI method.

Case	Material	Bead Name	Bead Type
a	PEG: Polyethylene glycol	OHC	SP2
		COC	SNa
b	PC: Poly hexamethylene carbonate diol	OHC	SP2
		CCC	SC1
		CC1	SC1
		CO3	SN0
c	DMF: Dimethylformamide	NCC	SN0
		HC=O	SNa
d	BD: 1,4-Butanediol	OHC	SP2
		CC1	SC1
e	HDI: Hexamethylene diisocyanate	NCO	SP3
		CC1	SC1

We performed energy minimization and equilibration simulations on 100 molecules of each material used for PU synthesis and compared the densities, in addition to the radius of gyration and end-to-end distance of polymers, obtained from atomistic and CG simulations with experimental values in SI (Table S3). Note that for atomistic simulation, we employed opls-aa force filed [36].

For synthesis, first, we mixed PC as macrodiol and HDI as isocyanate functional materials at 80 °C in the presence of DMF as solvent (50 w% solid content) in the simulation box. Then, the system is energy minimized using a steep integrator, equilibrated at room temperature and atmospheric pressure under NPT conditions using modified Berendsen thermostat and Parrinello-Rahman barostat. After reaching the equilibrium state, the reaction between OH and NCO from macrodiol and isocyanate, respectively, started in a stepwise manner, i.e., each step of reaction simulation followed by a considerable longer step of relaxation simulation [35]. We considered a 0.4±10% nm reaction cut-off for OH and NCO beads such that for beads fall into this cut-off, there is a probability for reaction to take place and outside of this cut-off no

reaction will take place[37]. After finding potential OH and NCO beads within the cutoff, the program converts them to urethane beads, named UOH and UNCO, respectively. The topology file was updated accordingly with the new added bonded potentials. It is worth emphasizing that relabeling the OH and NCO to UOH and UNCO beads immediately after each reaction takes place, prevents occurring of multiple reactions between NCO and OH groups, as it stands in real condition. When all hydroxyl groups, the OH beads, reacted with isocynate groups, the NCO beads, BD was added to the reaction mixture as the chain extender and chemical reaction between hydroxyl groups of BD and the remaining isocyante groups of HDI was started. We continued the reaction simulation loop until the conversion of about 97-98 % is reached. As considered in experiment, some part of PC were replaced by PEG (at 10%, 20% and 30% of weight ratios, see *Table 1*) in our simulations and similar simulation reaction was considered for these systems as well. Note that in these cases, the mixture of PEG and PC, as macrodiols, was added from the beginning of the reaction. Similar to the experimental synthesis, we removed the unreacted small species from the material after completion of simulation synthesis.

4.2 Characterization simulations

We estimated molecular weights and microphase separation for different PU systems, during and after polymerization. We designed a new analysis tool, similar to a size-exclusion chromatography, to study the M_n, M_w and PDI. Therefore, we were able to perform real-time size-exclusion characterization simulations. By employing this technique, we showed the organization of different diols in individual PU chains, as well as the structure heterogeneity of PU systems.

Results and Discussion

1. Experimental

We performed FTIR spectroscopy of PEG based polyurethanes, in order to verify the synthesis as well as understand the microphase organization of PU. The result is shown in *Figure 3*. Absence of any peak at 2270 cm^{-1} confirms the total reaction of isocyante groups in all the samples[38, 39]. NH bending vibration is also present[40]. The intensity of peak at 1110 cm^{-1} assigned to stretching vibration of C-O-C etheric bond shows an increase with increasing PEG content, as expected [21, 39, 41]. Absence of peaks at 3440 cm^{-1} (free NH)[42] indicates that all NH groups are participated in Hydrogen bonding interaction (3320 cm^{-1})[43]. NH can participate in H-bonding interactions with both carbonyl groups of polycarbonate and urethane and also etheric group of PEG[21]. Moreover, the average molecular weights of the synthesized PUs measured by GPC, see *Table 3*, confirm the formation of relatively high molecular weight thermoplastic polyurethanes with a fair molecular weight distribution. It is worth indicating that these values are obtained after purification of samples from unreacted and very low molecular weight materials.

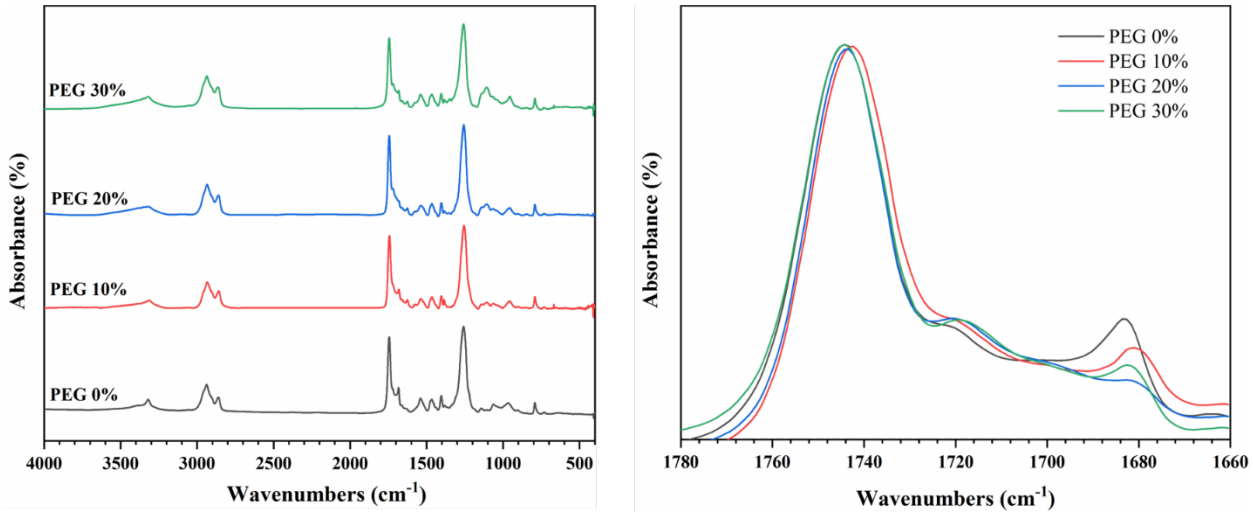

Figure 3. FTIR spectra of PEG-based PUs at different concentrations of PEG and zoom of carbonyl region.

There is a common method to evaluate hydrogen bonding in PU systems, so that, the peaks associated with carbonyl group is deconvoluted into different contributions[44]. Therefore, we studied the carbonyl region, shown in *Figure 3*, and quantified the contribution of different areas by deconvoluting peaks, see *Table 4*. Note that the deconvolution and fitting process is reported in SI in full detail (Figure S1). There are mainly four types of carbonyl in polycarbonate based PUs: Free and H-bonded carbonyl of carbonate, and free and H-bonded carbonyl of urethanes[19]. H-bonded carbonyl of urethanes can be both in ordered (crystalline) and disordered (amorphous) conformations[43]. Free carbonyl of carbonate appears at 1744 cm^{-1}. The peak at 1720 cm^{-1} could be both related to H-bonded carbonyl and also free carbonyl of urethanes. Peaks appeared at 1700 and 1680 cm^{-1} are assigned to disordered and ordered H-bonded carbonyl of urethanes, respectively[43, 45]. As it is clear in *Figure 3*, the intensity of 1680 cm^{-1} decreases by incorporation of PEG; therefore, one expects less H-bonded crystalline urethanes as PEG content increases, see *Table 4*. Thus, it is clear that by incorporation of PEG there is less self-association of H-bonded urethanes. Considering the fact that the H-bonded NH vibration is not influenced by the incorporation of PEG, one could rationalize it to be related to the fact that polar ether groups in PEG interact well with polar urethane groups, and there is more phase mixing between soft and hard segments as also similar evidences have been reported due to PEG incorporation in polyether based polyurethanes, before[21].

Table 3. GPC molecular weights of the synthesized PUs.

Sample	M_n (g/mol)	M_w (g/mol)	PDI (M_w/M_n)
PEG 0%	54883	74801	1.36
PEG 10%	56838	79166	1.39
PEG 20%	53765	73532	1.37
PEG 30%	51240	73056	1.43

Table 4. Area of deconvoluted peaks in carbonyl region.

Wavenumbers (cm^{-1})	Area (%)			
	PEG 0%	**PEG 10%**	**PEG 20%**	**PEG 30%**
1743	22.32	21.5	20.74	22.42
1720	3.76	4.07	4.33	3.99
1700	3.36	2.9	3.45	3.28
1680	5.06	3.93	2.52	3.32

So far, FTIR analysis indicated that a phase mixing between PEG and urethane groups occurs, as the PEG content increases. Therefore, to verify this observation, we further investigated the microphase structure of all PUs by AFM measurement. Phase and topographic images are shown in *Figure 4*. As expected, the incorporation of PEG changes the surface phase image of the PUs. More phase mixing between the hard and soft segments is observed by PEG incorporation. PUs containing 10% and 20% PEG have quite similar structure, while the system with 30% of PEG, exhibits filament-like structure. The micro-domain size also clearly decreases as a result of increasing PEG content, which is due to more phase mixing between soft and hard segments.

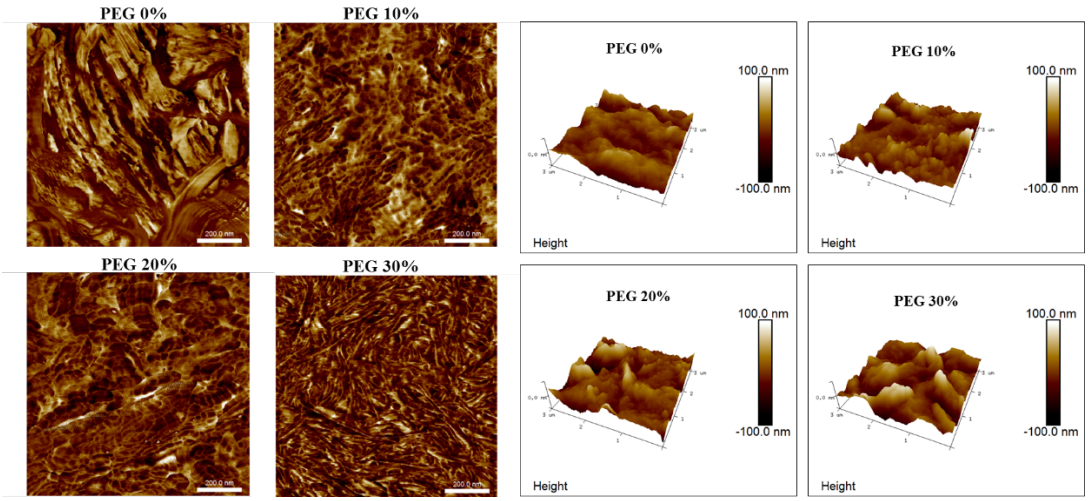

Figure 4. AFM images of synthesized PUs.

Table 5. Roughness of PUs containing PEG.

Sample	R_q (nm)	R_a (nm)
PEG 0%	16.8	13.7
PEG 10%	18.4	13.8
PEG 20%	23.1	16.9
PEG 30%	24.5	18.9

To evaluate the surface roughness, the root-mean-square (RMS) height deviation *Rq* is a common value to measure[44]. As clearly is evident in *Table 5* and the topographic images in *Figure 4*, the incorporation of PEG leads to a higher surface roughness. It is worth noting that similar trend has been observed for other systems [46, 47]. Thus, on the one hand, the surface roughness increases for higher PEG content PUs, and on the other hand, the FTIR results and AFM phase images clearly indicate a phase mixing between PEG

and urethane groups. Nevertheless, one would expect the formation of a smoother surface as a result of hard/soft phase mixing in PU, unless another concurrent phase separation, e.g., for PC and PEG, occurs.

Thermal behavior of the synthesized PUs was studied by DSC and DMTA, by which the T_g, melting points and crystallinity of different PU segments were measured. The thermograms are depicted in *Figure 5* and the melting points and T_g values are summarized in *Table 6*. As shown, the T_g of soft segment decreases by increasing PEG content due to the lower T_g of PEG as compared to PC[46, 48]. The first melting point in DSC graph is related to PEG as this peak intensifies by increasing PEG amount and the second endothermic peak is related to PC. Appearance of two melting peaks indicates the presence of segregated crystalline domains of PEG and PC. Combining this observation with FTIR and AFM results, it is clear that there is a microphase separation between PEG and PC within the soft domain [47]. This is also verified by the formation of a shoulder on the tan δ peak in DMTA graphs, as PEG content increases, i.e., PEG 20% and PEG 30%, see *Figure 5*. Moreover, for PEG 0%, there is a second T_g appeared in DSC thermogram at around 102 °C, which is related to the hard segment relaxation. Appearance of two T_g's for soft and hard segments, could be related to a large scale micro phase separation of these segments in PU and as PEG content increases, the phase mixing between PEG and urethane groups leads to disappearance of it.

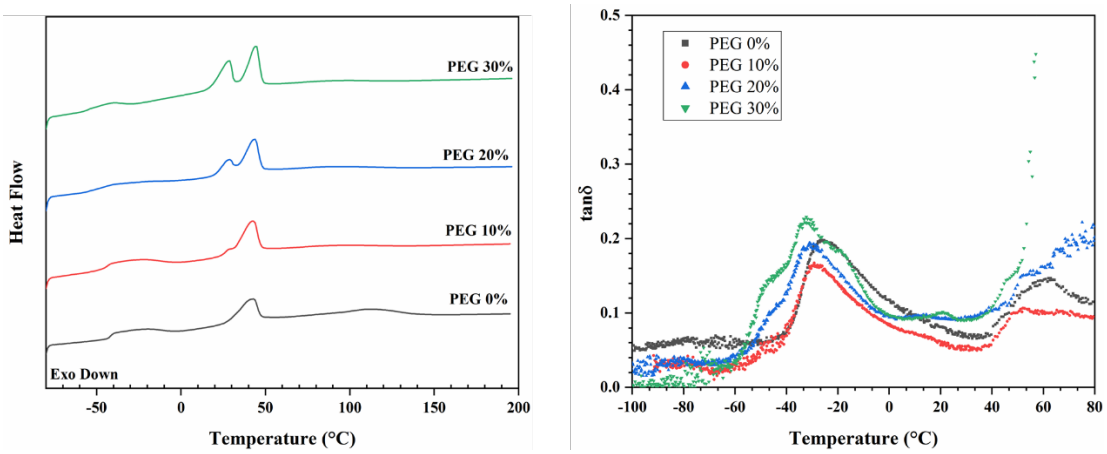

Figure 5. DSC and DMTA thermograms of the synthesized PUs with different PEG contents (second heating run for DSC).

Table 6. Melting point and Tg values for different PEG contents.

Sample	Tm_{PEG} (°C)	Tm_{PC} (°C)	Tg_s (°C)	Tg_h (°C)	Tg (°C) (based on DMTA data)
PEG 0%	-	41	-41.8	102.2	-24.8
PEG 10%	28	43	-43.8	-	-27.6
PEG 20%	27	44	-45.1	-	-29.8
PEG 30%	27	44	-55.2	-	-31.1

As already seen, all the synthesized PUs are semi-crystalline; therefore, the degree of crystallinity (X_c) could be calculated using equation 1[49]:

$$X_C = \frac{\Delta H_f}{w_{ss} \times \Delta H_f^0} \times 100\% \qquad \textit{Equation 1}$$

where ΔH_f is the experimental melting enthalpy of PUs, w_{ss} is the theoretical mass fraction of the soft segment. ΔH^0_f is the enthalpy of 100% crystalline PC (136 J g^{-1})[49] and 100% crystalline PEG (205 J g^{-1})[50]. The results are summarized in *Table 7*. As shown, both PEG, PC and total crystallinity is increasing by PEG incorporation. There is another interesting point that by increasing PEG content to 30%, the PC crystalline domains rapidly grows. This indicates that larger PEG crystalline domains induces larger PC crystalline domains. On the other word, the degree of phase separation between PC and PEG reaches higher values for samples containing more PEG.

Table 7. Calculated crystallinity from DSC data for PEG containing PUs.

Sample	PC Crystallinity %	PEG Crystallinity %	Total Crystallinity %
PEG 0%	9.03	-	9.03
PEG 10%	10.99	0.89	11.88
PEG 20%	8.21	11.34	21.55
PEG 30%	18.21	15.51	33.72

To reveal the crystalline structure of PUs, XRD was also employed. As shown in *Figure 6*, since both PEG and PC exhibit diffraction peaks at the same 2θ (20.2 and 23.6)[51], it is not possible to distinguish them in XRD patterns. After deconvolution of the crystalline and amorphous peaks, the crystallinity degree was calculated from the area ratio between intensity of the crystalline peaks to the total crystallinity, according to the Equation 2 [52]. The calculated crystallinity by XRD tabulated in *Table 8*, also shows that the total crystallinity increases by increasing PEG content. The values are in a good agreement with DSC data.

$$\%Crystallinity = \frac{area\ under\ crystallline\ peaks}{total\ area\ under\ all\ peaks} \times 100\% \qquad \textit{Equation 2}$$

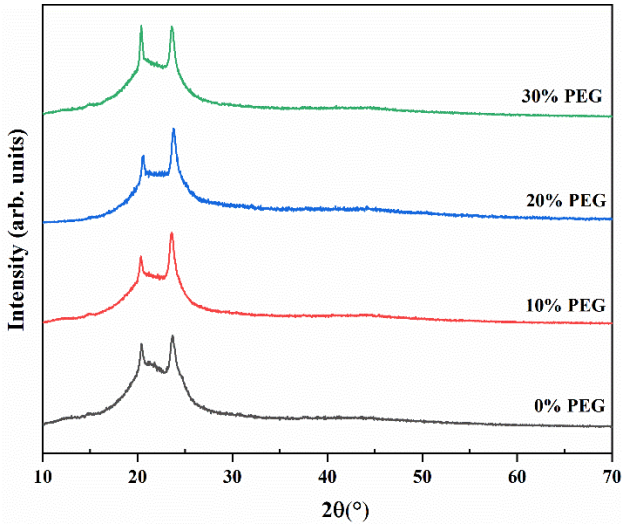

Figure 6. XRD of the synthesized PUs with different PEG contents.

Table 8. Crystallinity degree calculated from XRD for PUs.

Sample	Crystallinity degree %
PEG 0%	8.59
PEG 10%	11.53
PEG 20%	14.83
PEG 30%	25.49

All in all, based on the experimental analyses, one could conclude that by incorporation of PEG, a superhydrophilic polymer, into the PC, a hydrophobic polymer, the phase mixing between PEG and urethane group and phase separation between PEG and PC segments is expected to occur, concurrently. Therefore, one expects a patterned surface with varying wettability, combined of PC and PEG rich patches. However, no direct observation of such structure has been accomplished yet due to limited resolution of experiments when it comes to nano-scale measurements. It is worth noting that the density and physical properties of PC and PEG are rather similar and this makes it infeasible to distinguish them on the surface by means of indirect visualization techniques such as electron and scanning probe microscopy. Nevertheless, molecular simulations are versatile and reliable tools for this purpose; therefore, we employed a previously developed CG MD method[35] together with other mathematical analysis tools to visualize the phase organization of PEG and PC in nano-scale as well as in each individual PU chain.

2. Simulation

It is always interesting to visualize the arrangement of different molecules inside PU chains as the reaction proceeds. The first priority of simulation studies over experimental ones is the inherent ability of MD simulations for studying real-time properties in nano scale. As explained, we simulated the synthesis of all PU systems; therefore, we are able to visualize the nanophase organization of all materials at different stages of reaction. *Figure 7* shows the nanophase separation for PEG 0% and PEG 30% at different conversions, i.e., 10%, 70% and final conversion. The conversion is calculated based on the limiting reactant (OH groups) and the dimension of simulation boxes are about $80\times4\times9$ $(nm)^3$. This Figure shows the top view of the simulation boxes. It is obvious that the number of unreacted OH and NCO (Cyan beads) decreases as the reaction proceeds, for both cases. The phase separation between PEG and PC is considerable from the beginning of the reaction, i.e., 10% conversion, which is related to their inherent incompatibility and this phase separation remains more-or-less steady until the end of the reaction. This observation indicates that the phase separated domains of PEG and PC, which we have distinguished by DSC, presents from the initial stage of the reaction. In fact, the reaction takes place in a rather inhomogeneous condition when both PEG and PC are present.

For PEG 0% system, one could recognize the formation of domains rich of hard segments, see the red circle in the final conversion, which is in line with our observation from AFM and FTIR analysis. Looking at PEG 30% simulation, as reaction conversion increases, there are more aggregation of urethane segments around PEG domains. This has been observed by FTIR analysis and most likely is due to more polar nature of PEG and urethane groups. These groups are susceptible for formation of H-bond. Although, it is not possible to perform H-bond analysis for our CG simulations, we believe that combining FTIR analysis with this observation, indicates the formation of mixed PEG/urethane domains such that PEG domains are located at the interface of urethane groups. Apparently, this phenomenon leads to formation of a core-shell

like morphology such that the core consists of the superhydrophile PEG and urethane groups form the shell around it. The urethane shell separates the PEG domains from the continuous PC domain.

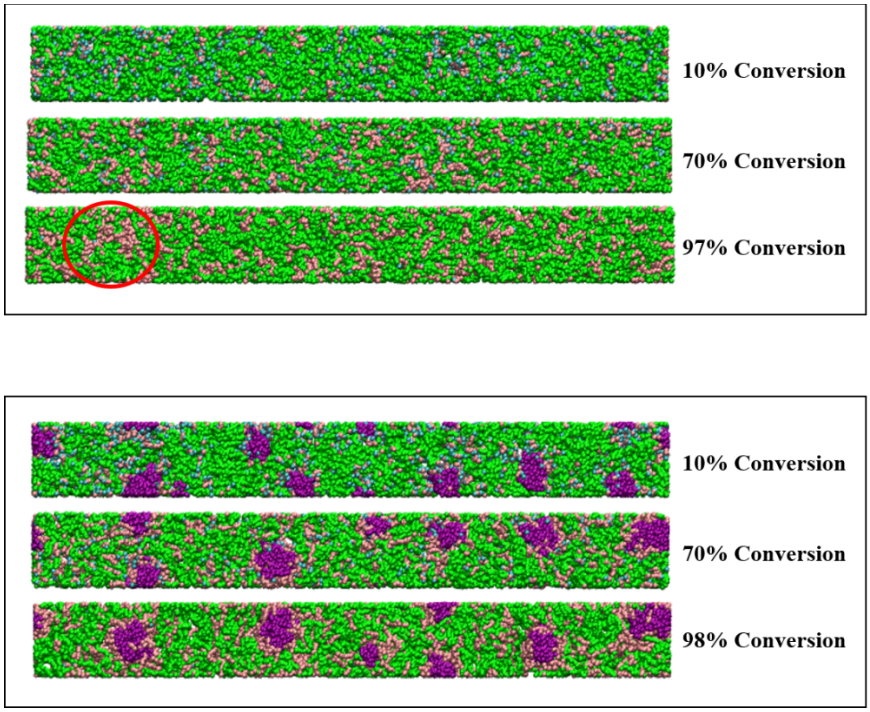

Figure 7. Structure arrangement (top view) at different conversion for PEG 0% (up) and PEG 30% (down). PC and PEG are depicted by green and purple dots, respectively. Hard segments are depicted by pink dots. Cyan beads are unreacted NCO and OH.

Structure arrangement at final conversion for PUs containing different amounts of PEG are depicted in *Figure 8*. As the PEG content increases, the PEG domains become larger and surrounded by a thicker layer of urethane groups. This is a very important observation and in good agreement with the experimental crystallinity measurements. In fact, one could tune the size of superhydrophile domains by controlling the PEG content fed to the reaction.

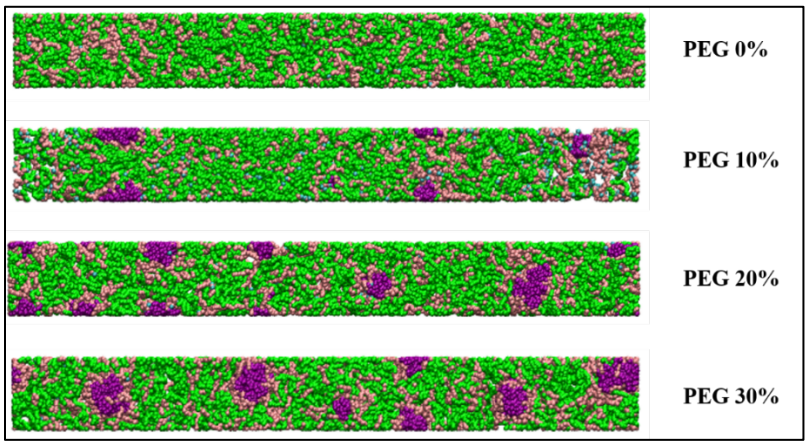

Figure 8. Structure arrangement (top view) at final conversion for PUs containing different amounts of PEG. PC and PEG are depicted by green and purple dots, respectively. Hard segments are depicted by pink dots. Cyan beads are unreacted NCO and OH.

Number and weight average molecular weights as a function of reaction conversion is shown in *Figure 9*. As expected, the molecular weight increases exponentially by increasing reaction conversion. After 90% of conversion, the rate of molecular weight increasing is higher in PU containing PEG. Also, the isocynate peak in FTIR (as a criterion for reaction termination) was disappeared sooner in the samples containing PEG in experimental reactions. This could be related to the higher level of flexibility of PEG as compared to PC, which makes the hydroxyl groups more available for urethane reactions. There is one point about calculating the final molecular weights regarding the purification of final samples from unreacted and low molecular weight materials. Similar to the experiment, we removed these impurities at the final conversion and calculated M_n and M_w for these conversion points. The results are shown in *Figure 9* and *Table 9*, as well. The molecular structures after purification is shown in SI (Figure S2). Note that this material removal has only been done for the last conversion point, therefore, there are two data points shown in *Figure 9* for the final conversions. The solid and open dot represent the molecular weights with and without purification process, respectively. The results are in good agreement with the experimental molecular weights obtained by GPC.

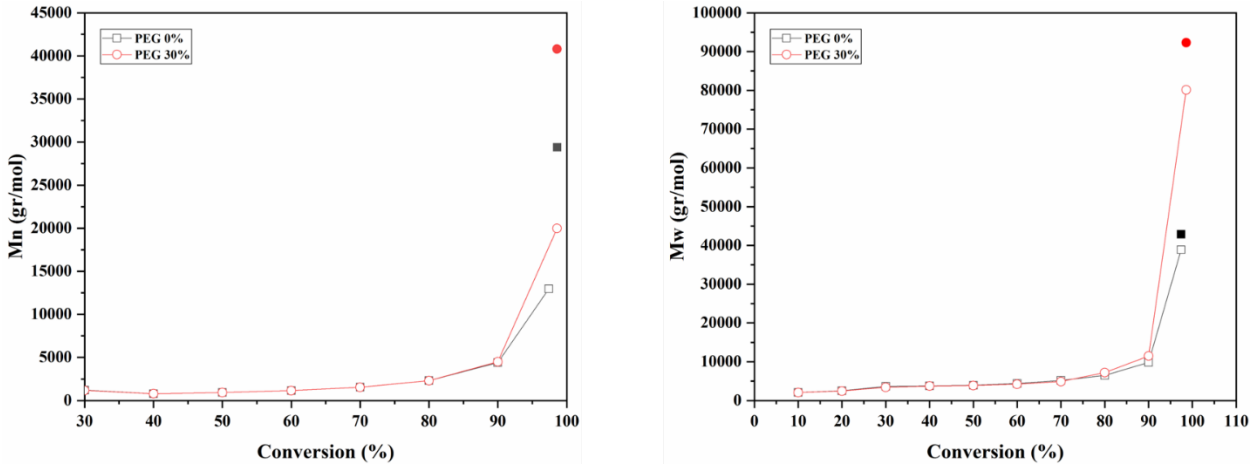

Figure 9. Number and weight average molecular weight as a function of reaction conversion.

Table 9. Molecular weights estimated by molecular dynamics simulation.

Sample	M_n (g/mol)	M_w (g/mol)	PDI (M_w/M_n)
PEG 0%	~29400	~42900	~1.5
PEG 30%	~40800	~92300	~2.3

So far, simulation results were in good agreement with experimental analysis. Moreover, the simulation visualizations showed that not only the PEG-rich domains phase separate from PC rich domains, but also they form a core-shell structure in which the PEG-rich regions form the core and urethane groups migrate to the interface of PEG-rich regions and form the shell structure. Next, we were interested in if, for instance, these PEG-rich domains are aggregation of PEG segments from different PU chains containing PEG and PC, or there are PEG-rich chains aggregated in these domains. On the other word, it is highly interesting to figure out that the phase separation between PEG and PC from the beginning of the reaction leads to a group of PU chains rich in PEG and a group of PU chains rich in PC or a random conformation of PEG and PC are present in all PU chains. In addition, it seems especially interesting to visualize the evolution of the molecular structure as the reaction proceeds. Therefore, we performed our size exclusion characterization

analysis [35] by which one is able to visualize the connectivity and the sequence of placement of different segments in individual PU chains. The results for PEG 0% and PEG 30% are illustrated in *Figure 10* and *Figure 11*, respectively.

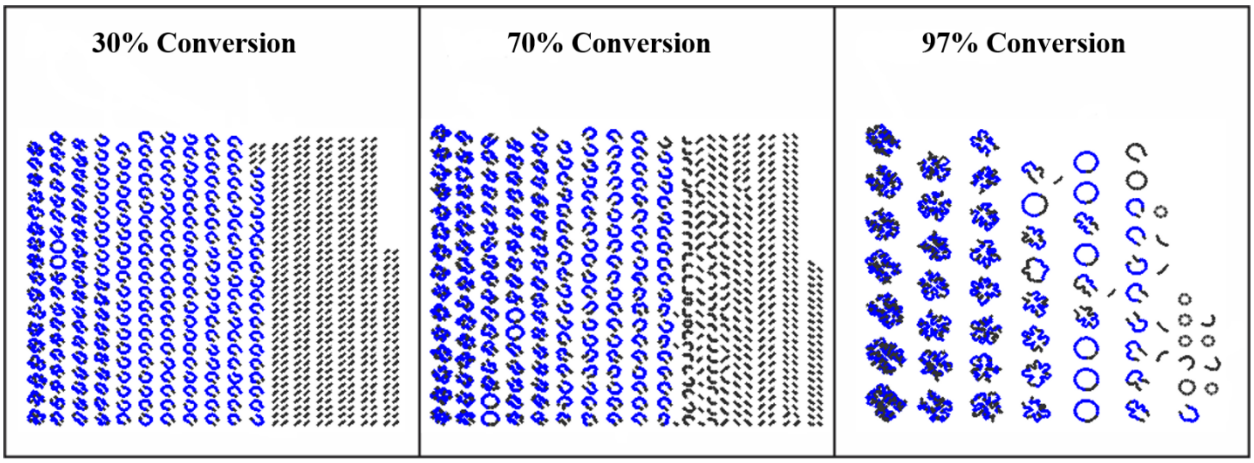

Figure 10. Molecular structure for PEG 0% at 30%, 70% and 97% conversion. PC is represented in blue.

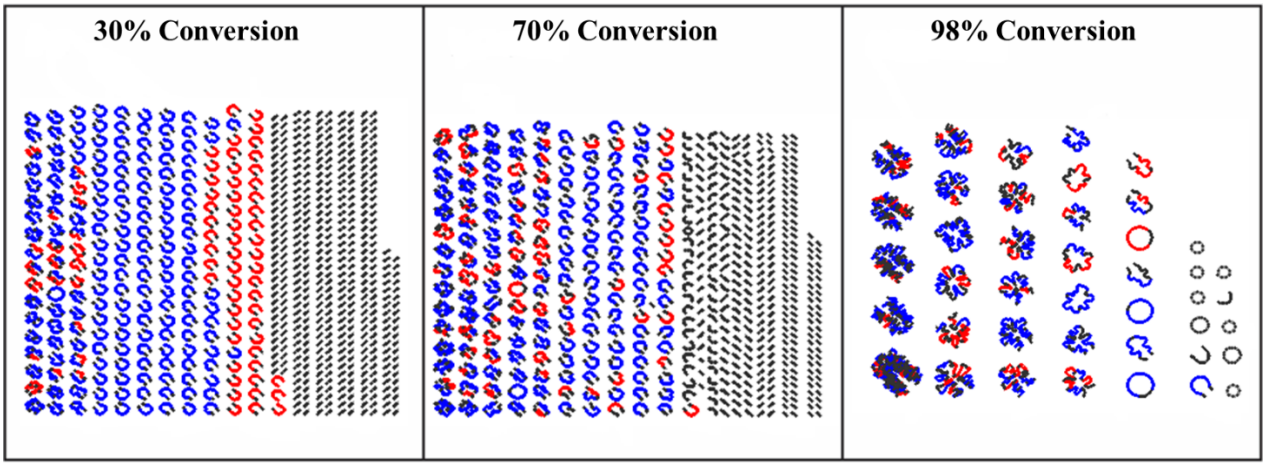

Figure 11. Molecular structure for PEG 30% at 30%, 70% and 97% conversion. PC and PEG are represented in blue and red, respectively.

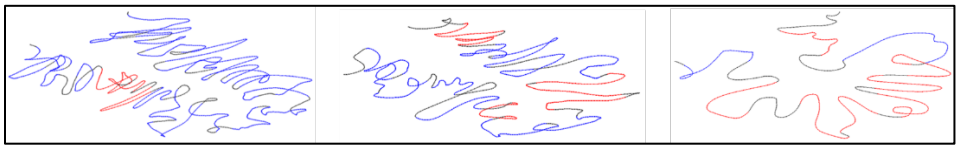

Figure 12. Molecular structure of selected chains in PEG 30%. PC and PEG are represented in blue and red, respectively.

As the reaction proceeds, more chains are bonded to each other and total number of chains decreases. The lower final molecular weight of PEG 0% might be related to the larger number of loops, see *Figure 11* at final conversion, which are unable to react with other functional groups. For PEG 30%, PEG and PC started to grow in size mainly in separated chains, so that, up to 30% conversion PEG-rich and PC-rich chains are present, see *Figure 11* at 30% conversion. After conversion reaches higher values, these PEG-rich and PC-

rich chains connected to each other and form larger PU chains consist of both PEG and PC domains. However, these PU chains mainly consist of large blocks of PEG and PC segments, see *Figure 12*. This explains the reasons of formation of urethane groups at the interface of PEG and PC. In fact, the NCO groups migrate to the interface of PEG and PC, where most of unreacted OH groups are available; therefore, the formation of urethane groups in that region is significant and the possibility of formation of H-bond with PEG segments increases.

All in all, our CG MD simulation results are in good agreement with experimental evidences such that distinct domains of PEG and PC, which are connected by the urethane groups, are recognized. As the higher PEG content exist, the more urethane groups migrate to the interface of PEG and PC and form a core-shell structure. The core consists of the superhydrophilic domain and the disperse medium, i.e., PC, forms the hydrophobic domain.

Conclusion

Thermoplastic PUs, based on polycarbonate diol were synthesized with and without PEG in different concentrations. The effect of introducing PEG into the backbone of PU was investigated by both experimental and simulation studies. FTIR confirmed the PU formation and PEG insertion. It also indicated that there is a phase mixing between soft and hard segments due to compatibility between PEG and hard segment. AFM confirmed this phase mixing and higher roughness due to PEG incorporation. Inherent incompatibility between PEG and PC caused a phase separation between two soft segments. Thermal and thermo-mechanical analyses also indicated a clear distinct crystalline structure for PEG and PC. A distinct relaxation behavior, as appeared in tan δ graphs, reconfirmed the formation of separated domains, i.e., PEG-rich and PC-rich regions, in PU morphology. Based on DSC and XRD data, PEG increasing made more phase separated crystalline domains of PEG and PC. We also performed CG MD simulations to be able to complete our picture from perspectives that experiment is not capable of visualizing. The simulation results confirmed the above observations as well. They give us the ability to visualize the nano structure of all systems that was not possible in experiment due to the similarity of the physical properties of PEG and PC domains. A core-shell liked structure in which the urethane groups form the shell by aggregating around the PEG-rich regions, not only explained the H-bond between PEG and urethanes but also verified the successful synthesis of a patterned structure with varying wettability on the PU surface. Having time dependent simulations done, we were able to study the real-time morphology of PU systems as a function of conversion of the reactions. We learned that PEG/PC phase separation occurs simultaneously after mixing and the reaction takes place in an inhomogeneous medium. Therefore, the presence of urethane groups at the interface of PEG and PC was rationalized. To summarize, we were successful to synthesize a novel amphiphilic self-assembled PU with phase segregated superhydrophilic and hydrophobic moieties and studied the evolution of phase separation with molecular dynamics simulation. Our method gives an easy-fabricating and versatile rout for production of patterned surface with varying wettability in which one could control the size of superhydrophilic moieties by the weight ratio of PEG fed to the reaction.

Acknowledgements

The authors would like to thank Iran National Science Foundation (INSF) and Diputación Foral de Gipuzkoa for financial support.

References

[1] by Robin H A Ras and A. Marmur, *Non-wettable Surfaces: Theory, Preparation and Applications*, 1st ed. RSC Soft Matter No. 5, 2017.

[2] Inseong You, Nayeon Yun, and H. Lee, "Surface-Tension-Confined Microfluidics and Their Applications," *ChemPhysChem,* vol. 14, pp. 471 – 481 2013.

[3] Takahiro Ishizaki, N. Saito, and O. Takai, "Correlation of Cell Adhesive Behaviors on Superhydrophobic, Superhydrophilic, and Micropatterned Superhydrophobic/Superhydrophilic Surfaces to Their Surface Chemistry," *Langmuir,* vol. 26, no. 11, pp. 8147–8154, 2010.

[4] Shunsuke Nishimoto *et al.*, "TiO2-based superhydrophobic–superhydrophilic patterns: Fabrication via an ink-jet technique and application in offset printing," *Applied Surface Science,* vol. 255, pp. 6221–6225, 2009.

[5] Hao Bai, Lin Wang, Jie Ju, Ruize Sun, Yongmei Zheng, and L. Jiang, " Efficient Water Collection on Integrative Bioinspired Surfaces with Star-Shaped Wettability Patterns," *Adv. Mater,* vol. 26, no. 5025–5030, 2014.

[6] X. L. Yu Wang, Heng Hu, Guojun Liu, and M. Rabnawaz, "Hydrophilically patterned superhydrophobic cotton fabrics and their use in ink printing," *J. Mater. Chem,* vol. 2, p. 8094, 2014.

[7] B. Chang *et al.*, "Capillary-driven self-assembly of microchips on oleophilic/oleophobic patterned surface using adhesive droplet in ambient air," *APPLIED PHYSICS LETTERS,* vol. 99, p. 034104, 2011.

[8] Lianbin Zhang, Jinbo Wu, Mohamed Nejib Hedhili, X. Yanga, and P. Wang, "Inkjet printing for direct micropatterning of a superhydrophobic surface: toward biomimetic fog harvesting surfaces," *Journal of Materials Chemistry A,* vol. 3, pp. 2844-2852, 2015.

[9] Arvind K. Singh Chandel, Chinta Uday Kumar, and S. K. Jewrajka, "Effect of Polyethylene Glycol on Properties and Drug Encapsulation−Release Performance of Biodegradable/Cytocompatible Agarose−Polyethylene Glycol−Polycaprolactone Amphiphilic Co-Network Gels," *ACS Applied Materials & Interfaces,* vol. 1, 2016.

[10] Li-Chong Xu and C. A. Siedlecki, "Microphase separation structure influences protein interactions with poly(urethane urea) surfaces," *Journal of Biomedical Materials Research Part A,* pp. 126-136, 2009.

[11] C. Prisacariu, *Polyurethane Elastomers: From Morphology to Mechanical Aspects*. Springer, 2011.

[12] J. R. Li-Chong Xu, Christopher A. Siedlecki, "Dynamics of hydrated polyurethane biomaterials: Surface microphase restructuring, protein activity and platelet adhesion," *Acta Biomaterialia,* no. 6, pp. 1938–1947, 2010.

[13] Si Lei Phua *et al.*, "Reinforcement of Polyether Polyurethane with Dopamine-Modified Clay: The Role of Interfacial Hydrogen Bonding," *ACS Applied Materials & Interfaces,* vol. 4, p. 8, 2012.

[14] S. L. Cooper and J. Guan, "Advances in Polyurethane Biomaterials," 2016.

[15] I. Yilgör, E. Yilgör, and G. L. Wilkes, "Critical parameters in designing segmented polyurethanes and their effect on morphology and properties: A comprehensive review," *Polymer,* vol. 58, pp. A1-A36, 2015.

[16] P. Kro´l, "Synthesis methods, chemical structures and phase structures of linear polyurethanes. Properties and applications of linear polyurethanes in polyurethane elastomers, copolymers and ionomers," *Progress in Materials Science,* no. 52, pp. 915–1015, 2007.

[17] E. Y. Iskender Yilgor, I. Guclu Guler, Thomas C. Ward, Garth L. Wilkes, "FTIR investigation of the influence of diisocyanate symmetry on the morphology development in model segmented polyurethanes," *Polymer,* no. 47, pp. 4105–4114, 2006.

[18] J. S. L. J. T. Garrett and J. Runt, "Microphase Separation of Segmented Poly(urethane urea) Block Copolymers," *Macromolecules,* no. 33, pp. 6353-6359, 2000.

[19] Rebeca Hernandez *et al.*, "A Comparison of Phase Organization of Model Segmented Polyurethanes with Different Intersegment Compatibilities," *Macromolecules,* no. 41, pp. 9767-9776, 2008.

[20] J. W. Rebeca Hernandez, Ajay Padsalgikar, James Runt, " Microstructural Organization of Three-Phase Polydimethylsiloxane-Based Segmented Polyurethanes," *Macromolecules,* vol. 40, pp. 5441-5449, 2007.

[21] T. G. G. ANN Z. OKKEMA, RICHARD J. ZDRAHALA, DONALD D. SOLOMON STUART L. COOPER, "Bulk, surface, and blood-contacting properties of polyetherurethanes modified with polyethylene oxide," *Journal of Biomaterials Science, Polymer Edition,* vol. 1, no. 1, pp. 43-62, 1989.

[22] Peiyu Sun *et al.*, "Facile Preparation of Mussel-Inspired Polyurethane Hydrogel and Its Rapid Curing Behavior," *ACS Appl. Mater. Interfaces,* vol. 6, no. 15, pp. 12495-12504, 2014.

[23] Shan-hui Hsu and Y.-C. Kao, "Biocompatibility of Poly(carbonate urethane)s with Various Degrees of Nanophase Separation," *Macromol. Biosci.,* no. 5, pp. 246–253, 2005.

[24] Taeyi Choi, Jadwiga Weksler, Ajay Padsalgikar, Rebeca Hernández, and a. J. Runt, "Polydimethylsiloxane-Based Polyurethanes: Phase-Separated Morphology and In Vitro Oxidative Biostability," *Aust. J. Chem.,* no. 62, pp. 794–798, 2009.

[25] A. Eceiza *et al.*, "Thermoplastic Polyurethane Elastomers Based on Polycarbonate Diols With Different Soft Segment Molecular Weight and Chemical Structure: Mechanical and Thermal Properties," *POLYMER ENGINEERING AND SCIENCE,* 2008.

[26] Rafael Bergamo Trinca and M. I. Felisberti, "Effect of diisocyanates and chain extenders on the physicochemical properties and morphology of multicomponent segmented polyurethanes based on poly(L-lactide), poly(ethylene glycol) and poly(trimethylene carbonate)," *Polym Int,* no. 64, pp. 1326–1335, 2015.

[27] C. Wenning, A. M. Schmidt, and M. C. Leimenstoll, "Reaction-induced phase separation in hexamethylene diisocyanate-based poly(propylene oxide)/poly(ethylene oxide) bi-soft segment oligomers," *Polym Int* no. 67, pp. 481–489, 2018.

[28] J. J. Zhonglin Luo, "Molecular dynamics and dissipative particle dynamics simulations for the miscibility of poly(ethylene oxide)/poly(vinyl chloride) blends," *Polymer,* no. 51, pp. 291–299, 2010.

[29] Y. V. K. Alexey A. Gavrilov, Pavel G. Khalatur, Alexander V. Chertovich, "Microphase separation in regular and random copolymer melts by DPD simulations," *Chemical Physics Letters,* no. 503, pp. 277–282, 2011.

[30] M. M. Kostas Ch. Daoulas, Juan J. de Pablo, Paul F. Nealeyb and Grant D. Smith, "Morphology of multi-component polymer systems: single chain in mean field simulation studies," *Soft Matter,* no. 2, pp. 573–583, 2006.

[31] E. Yildirim, M. Yurtsever, G.L. Wilkes, and I. Yilgor, "Effect of intersegmental interactions on the morphology of segmented polyurethanes with mixed soft segments: A coarse-grained simulation study," *Polymer,* no. 90, pp. 204-214, 2016.

[32] Xia Wang, Jingcheng Xu, Lingling Li, Yi Liu, Ying Li, and Q. Dong, "Influences of fluorine on microphase separation in fluorinated polyurethanes," *Polymer,* no. 98, pp. 311-319, 2016.

[33] Iman Sahebi Jouibari, Vahid HaddadiAsl, and M. M. Mirhosseini, "A novel investigation on micro-phase separation of thermoplastic polyurethanes: simulation, theoretical, and experimental approaches," *Iranian Polymer Journal* no. 28, pp. 237–250, 2019.

[34] Mohammad Masoud Mirhosseini, Vahid Haddadi-Asl, and I. S. Jouibari, "A simple and versatile method to tailor physicochemical properties of thermoplastic polyurethane elastomers by using novel mixed soft segments," *Mater. Res. Express,* vol. 6, p. 065314, 2019.

[35] H. M. Hassan Ghermezcheshme, Mohsen Mohseni, Morteza Ebrahimi, Gijsbertus de With, "MARTINI-based Simulation Method for Step-growth Polymerization and its Analysis by Size Exclusion Characterization: A Case Study of Cross-linked Polyurethane," *Physical Chemistry Chemical Physics,* 2019.

[36] S. J. Marrink, H. J. Risselada, S. Yefimov, D. P. Tieleman, and A. H. d. Vries, "The MARTINI Force Field: Coarse Grained Model for Biomolecular Simulations," *J. Phys. Chem. B,* no. 111, pp. 7812-7824, 2007.

[37] H. Makki *et al.*, "A simulation approach to study photo-degradation processes of polymeric coatings," *Polymer Degradation and Stability,* no. 105, pp. 68-79, 2014.

[38] J. P. e. Milena Špírková, Adam Strachota, Rafał Poreba, Oskar Bera, Ludmila Kaprálková, Josef Baldrian, Miroslav Šlouf, Nada Lazic, Jaroslava Budinski-Simendic, "Novel polycarbonate-based polyurethane elastomers: Composition–property relationship," *European Polymer Journal,* no. 47, pp. 959–972, 2011.

[39] Zhicheng Pan *et al.*, "Surface Distribution and Biophysicochemical Properties of Polymeric Micelles Bearing Gemini Cationic and Hydrophilic Groups," *ACS Applied Materials & Interfaces,* vol. 9, no. 3, 2017.

[40] Yan Zhang, Jianjun Liao, Xiangchen Fang, Fudong Bai, Kai Qiao, and L. Wang, "Renewable High-Performance Polyurethane Bioplastics Derived from Lignin–Poly(ε-caprolactone)," *ACS Sustainable Chem. Eng.,* vol. 5, no. 5, pp. 4276-4284, 2017.

[41] R.-x. Z. Ying Zhang, "Synthesis and in vitro drug release behavior of amphiphilictriblock copolymer nanoparticles based on poly (ethylene glycol) and polycaprolactone," *Biomaterials,* no. 26, pp. 6736–6742, 2005.

[42] Chunfeng Ma, Hao Zhou, Bo Wu, and G. Zhang, "Preparation of Polyurethane with Zwitterionic Side Chains and Their Protein Resistance," *ACS Appl. Mater. Interfaces,* vol. 3, no. 2, pp. 455-461, 2011.

[43] K. H. L. MichaelM. Coleman, Daniel J. Skrovanek and Paul C. Painter, "Hydrogen bonding in polymers, 4. Infrared Temperature studies of a simple polyurethane," *Macromolecules,* vol. 19, pp. 2149-2157, 1986.

[44] Chenyu Wang, Olga Yu Zolotarskaya, Kayesh M. Ashraf, Xuejun Wen, Dennis E. Ohman, and K. J. Wynne, "Surface characterization, antimicrobial effectiveness, and human ell response of a biomedical grade polyurethane blended with a mixed soft block PTMO-Quat/PEG copolyoxetane polyurethane," *ACS Applied Materials & Interfaces,* vol. 11, no. 23, pp. 20699-20714, 2019.

[45] B. Yang, W. M. Huang, C. Li, and L. Li, "Effects of moisture on the thermomechanical properties of a polyurethane shape memory polymer," *Polymer,* no. 47, pp. 1348–1356, 2006.

[46] H. Y. Fatemeh Shokrolahi, "Soft segment composition and its influence on phase-separated morphology of PCL/PEG-based poly(urethane urea)s," *Iran Polym J,* no. 23, pp. 505–512, 2014.

[47] J. P. J. a. N. Kumar, "Self Assembly of Amphiphilic (PEG)3-PLA Copolymer as Polymersomes: Preparation, Characterization, and Their Evaluation As Drug Carrier," *Biomacromolecules,* no. 11, pp. 1027–1035, 2010.

[48] Cancan Xu, Yihui Huang, Liping Tang, and Y. Hong, "Low Initial Modulus Biodegradable Polyurethane Elastomers for Soft Tissue Regeneration," *ACS Applied Materials & Interfaces,* vol. 9, no. 3, pp. 2169-2180, 2017.

[49] R. Zhu *et al.*, "Influence of hydroxyl-terminated polydimethylsiloxane on high-strength biocompatible polycarbonate urethane films," *Biomed Mater,* vol. 12, no. 1, p. 015011, Dec 9 2017.

[50] LI ZHAO, WEIHUA KAI, YONG HE, BO ZHU, and Y. INOUE, "Effect of Aging on Fractional Crystallization of Poly(Ethylene oxide) Component in Poly(Ethylene oxide)/Poly(3-hydroxybutyrate) Blends," *Journal of Polymer Science: Part B: Polymer Physics,* vol. 43, pp. 2665–2676, 2005.

[51] Rongrong Liu, Qian Zhang, Qian Zhou, Ping Zhang, and H. Dai, "Nondegradable magnetic poly (carbonate urethane) microspheres with good shape memory as a proposed material for vascular embolization," *Journal of the Mechanical Behavior of Biomedical Materials,* vol. 82, pp. 9-17, 2018.

[52] Maryam Safari, Leila Naji, Richard T. Baker, and F. A. Taromi, "Influence of electrolytes of Li salts, EMIMBF4, and mixed phases on electrochemical and physical properties of Nafion membrane," *J. APPL. POLYM. SCI.,* vol. 134, no. 35, p. 45239, 2017.